

Single-walled carbon nanotubes oust graphene and semiconductor saturable absorbers in Q-switched solid-state lasers at 2 μm

Xavier Mateos,^{1,2,*} Pavel Loiko,³ Sun Young Choi,⁴ Fabian Rotermund,⁵ Magdalena Aguiló,¹ Francesc Díaz,¹ Uwe Griebner² and Valentin Petrov²

¹Física i Cristal·lografia de Materials i Nanomaterials (FiCMA-FiCNA)-EMaS, Dept. Química Física i Inòrganica, Universitat Rovira i Virgili (URV), Campus Sescelades, E-43007 Tarragona, Spain

²Max-Born-Institute for Nonlinear Optics and Ultrafast Spectroscopy, 2A Max-Born-Str., 12489 Berlin, Germany

³ITMO University, 49 Kronverkskiy pr., 197101 St. Petersburg, Russia

⁴Department of Physics & Department of Energy Systems Research, Ajou University, San 5 Wonchun-dong, 443-749 Suwon, Republic of Korea

⁵Department of Physics, KAIST, Daejeon 34141, Republic of Korea

*Corresponding author: xavier.mateos@urv.cat, mateos@mbi-berlin.de

Abstract The superior performance of a saturable absorber (SA) based on randomly-oriented single-walled carbon nanotubes (SWCNTs) operating in the spectral region of their first fundamental transition E_{11} over a graphene-SA containing several ($n = 3$) carbon layers and a commercial semiconductor SA (SESA) for passive Q-switching of bulk thulium solid-state lasers is demonstrated. Using SWCNT-SA in a compact diode-pumped Tm:KLuW laser, a maximum average output power of 1.36 W is achieved at 1932-1944 nm corresponding to a slope efficiency of 41% and pulse characteristics of 48 ns / 5.5 μJ which are superior to that for graphene-SA (123 ns / 3.1 μJ) and SESA (61 ns / 1.1 μJ). SWCNT-SAs are promising for eye-safe miniature lasers at $\sim 2 \mu\text{m}$ generating nanosecond pulses in the MHz repetition frequency range.

Keywords: saturable absorber; carbon nanotubes; graphene, semiconductor absorber; thulium laser.

1. Introduction

Solid-state lasers emitting at $\sim 2 \mu\text{m}$ (eye-safe spectral region) based on thulium (Tm^{3+}) or holmium (Ho^{3+}) ions [1] are of practical importance in medicine, sensing of CO_2 and water in the atmosphere (LIDAR) and metrology. A simple method to produce nanosecond (ns) pulses in such lasers is to introduce a nonlinear optical element showing saturable absorption in the range of the laser emission into the laser resonator. Such passively Q-switched (PQS) lasers benefit from compactness, all-solid design and the absence of external control. Their performance can be boosted when applying the microchip concept, with the active material and a saturable absorber (SA) both placed in a plano-plano cavity with its geometrical length determined by the thickness of the optical elements [2]. For PQS microchip lasers, besides high efficiency due to low intracavity losses, robust and insensitive to misalignment, one can expect the generation of very short pulses because of the reduced cavity roundtrip time [3].

Contrary to the $\sim 1 \mu\text{m}$ spectral range, for which well-developed commercial SAs exist, namely “slow” SAs based on transition-metal-doped dielectrics, e.g. Cr^{4+} :YAG [4-6], and “fast” SAs based on semiconductor structures [7,8], the search for proper SAs for passive Q-switching of Tm and Ho lasers is still ongoing. Here, “fast” and “slow” SAs are classified according to the relation between the recovery time of the initial absorption (τ_{SA}) and the characteristic time for the formation of a single Q-switched pulse (Δt), as $\tau_{\text{SA}} \ll \Delta t$ and $\tau_{\text{SA}} \geq \Delta t$, respectively. Note that for mode-locking completely different time scales apply and a “fast” SA for PQS lasers can be considered as a “slow” SA for mode-locked lasers. Accordingly, one speaks of saturation intensity or saturation fluence. At $\sim 2 \mu\text{m}$, “slow” SAs such as Cr^{2+} :ZnS and Cr^{2+} :ZnSe [9,10] suffer from low optical quality and low laser induced damage threshold (LIDT), and the technology of “fast” semiconductor SAs, although such are offered commercially, is far from being mature. Recently, carbon nanostructures, namely graphene – a single layer of carbon atoms arranged in a honeycomb lattice, and single-walled carbon nanotubes (SWCNTs) – rolled sheets of graphene, have attracted the attention of many researchers as broadband SAs for near-IR solid-state lasers [11-13]. These materials offer low saturation intensity, ultrafast recovery time of the initial absorption, reasonable LIDT and relatively simple fabrication methods. In addition, such nanostructures can be easily integrated in compact microchip lasers [14] by direct deposition on optical surfaces.

Besides graphene nanostructures, several types of “fast” nanostructured SAs for $\sim 2 \mu\text{m}$ lasers have been proposed to date. They include (i) glasses with semiconductor quantum dots (QDs), e.g. PbS [15]; (ii) few-layer transition-metal dichalcogenides (TMDs), namely MoS_2 , WS_2 , etc. [16,17], (iii) topological insulators (TIs), namely Bi_2Se_3 , etc. [18], (iv) few-layer black phosphorus (BP) [19], and (v) graphene oxide [20]. QD-doped glasses suffer from strong absorption at the pump wavelength, glass non-uniformity and low thermal conductivity. The remaining SAs are typically produced as thin films containing individual few-layer flakes of the material and suffers high non-saturable losses, low LIDT and poor environmental stability. Thus, in the present study, we exclude these materials from the comparison.

The performance of graphene- and SWCNT-SAs in mode-locked lasers has been thoroughly addressed to date both at ~ 1 and $\sim 2 \mu\text{m}$ [21,22] resulting in generation of fs pulses making these materials competitive to the GaSb-based semiconductor saturable absorber mirrors (SESAMs). Still, the perspectives of graphene nanostructures for $\sim 2 \mu\text{m}$ PQS oscillators remain unclear. Even though several papers have been published about graphene-SAs, see [14,23,24] and Refs. therein and only few – on the SWCNT-SAs [25,26] for PQS $\sim 2 \mu\text{m}$ lasers, no direct comparison of different types of SAs has been performed. In the present letter, we report on such a comparison of $\sim 2 \mu\text{m}$ lasers PQS by SWCNT-, graphene- and commercial semiconductor-SAs. The results demonstrate, for the first time to the best of our knowledge, the superior performance of SWCNT SAs.

2. Laser set-up

The active element (AE) was prepared from monoclinic 5 at.% Tm:KLu(WO₄)₂ (Tm:KLuW) grown by the TSSG method and cut along the N_g -axis [27]. This crystal is known for its advantageous spectroscopic properties for efficient continuous-wave and pulsed laser operation at $\sim 2 \mu\text{m}$ [28]. The 3.5 mm-thick AE was polished to laser quality, wrapped into indium foil and mounted in a Cu-holder water-cooled down to 12 °C. The plano-plano laser cavity comprised a flat pump mirror (PM), antireflection (AR) coated for 0.78-1.0 μm and high-reflection coated for 1.84-2.1 μm , and a flat output coupler (OC) with a transmission of 10% at the laser wavelength. The transmission-type SA was inserted between the AE and OC. All the optical elements in the cavity were placed next to each other minimizing the air gaps. The AE was pumped through the PM with a fiber-coupled AlGaAs laser diode (fiber details: core diameter: 200 μm , numerical aperture, N. A. = 0.22) emitting unpolarized radiation at $\sim 802 \text{ nm}$ (the emission wavelength stabilized by water-cooling) using a lens assembly (1:1 reimaging ratio, 30 mm focal length). The pump spot radius w_p in the crystal was 100 μm (confocal parameter, $2z_R = 1.73 \text{ mm}$, M^2 factor of the pump beam: ~ 86). The radius of the laser mode w_L in the crystal and at the SA was calculated with the ABCD method using the parameters of the thermal lens from [27] to be $70 \pm 5 \mu\text{m}$. The total absorption of the pump radiation under lasing conditions was 73%.

3. Saturable absorbers

Three SAs were employed for passive Q-switching of the compact (microchip-type) Tm:KLuW laser, namely, home-made SWCNT- and graphene-SAs and a commercial transmission-type semiconductor-SA (SESA), see table 1 for parameters and figure 1 for the small-signal absorption spectra and images of the SAs. The SWCNT-SA was fabricated such that the saturable absorption ($\alpha'_S = 0.55\%$) was similar to that of the commercial SESA ($\alpha'_S = 0.50\%$). The graphene-SA contained several ($n = 3$) carbon layers in order to increase α'_S , however, increasing the number of layers is limited by the fast increase of the scattering in the layer-to-layer interfaces for large n , so the resulting α'_S was $\sim 0.24\%$.

The characteristics of the SWCNT-SA are summarized in figure 2. The SWCNTs were synthesized by the arc-discharge technique (Meijo nano Carbin). The prepared SWCNT / PMMA solution was spin-coated onto an uncoated quartz substrate (film thickness: $\sim 300 \text{ nm}$, substrate thickness: 1 mm) [13,29]. By controlling the concentration of SWCNTs and the thickness of the film, it was possible to adjust α'_S of the SA as mentioned above. Individual SWCNTs, figure 2(a), well distributed in the film were randomly oriented (spaghetti-like). The broad absorption band centered at $\sim 1.9 \mu\text{m}$ for the SWCNT-SA, figure 2(b), is related to the first fundamental transition, E_{11} , of semiconducting nanotubes with slightly different diameters from 1.5 to 2.2 nm. In agreement with the simplified scheme of the electronic state density for the carbon nanotubes, figure 2(c), the E_{11} optical transition corresponds to the excitation of electrons from the highest sub-band v_1 of the valence band to the lowest sub-band c_1 of the conduction one where v_1 and c_1 sub-bands appear due to the van Hove singularities of 1D semiconducting nanotubes [30]. The study of the SWCNT-SA with a pump-probe method at 1920 nm revealed the absorption saturation effect with a double-exponential recovery which was fitted by two characteristic times of $\sim 250 \text{ fs}$ and 1.16 ps [22]. The small-signal absorption of the SWCNT-SA at the laser wavelength α' was 2.45%, the fraction of the saturable losses $\alpha'_S/\alpha' = 0.206$ and the estimated saturation intensity at $\sim 2 \mu\text{m}$, $I_{\text{sat}} = 7 \pm 1 \text{ MW/cm}^2$ [29].

The graphene used in this work was synthesized by chemical vapor deposition (CVD) on Cu foil employing a mixture of methane and hydrogen gases. The graphene layers were transferred onto the surface of a 1-in. quartz substrate (1 mm-thick), see figure 1(d), using layer-by-layer stacking process. For the graphene-SA, α' at the laser wavelength was 5.70%,

$\alpha'_s/\alpha' = 0.042$ and the estimated saturation intensity at $\sim 2 \mu\text{m}$, $I_{\text{sat}} = 1 \pm 0.2 \text{ MW/cm}^2$ [29]. The measured recovery times at $\sim 1.04 \mu\text{m}$ were 200 fs and 1.5 ps [21].

The commercial transmission-type SESA on a GaAs substrate (625 μm -thick, BATOP) was AR-coated around $2 \mu\text{m}$ and mounted on a Cu-holder, figure 1(b). Its small-signal absorption at the laser wavelength α' was 1.10%, the fraction of the saturable losses $\alpha'_s/\alpha' \sim 0.50$ and the provided saturation fluence, $F_{\text{sat}} = 300 \mu\text{J/cm}^2$ ($I_{\text{sat}} = 23 \text{ MW/cm}^2$). The provided recovery time of the SESA was 13 ps.

4. Results and discussion

Stable Q-switching was achieved with all three studied SAs. The corresponding input-output dependences are shown in figure 3(a). Power-scaling was limited by Q-switching instabilities due to heating of the SA by residual (non-absorbed) pump [14] but no other detrimental thermal effects were detected. The laser output was linearly polarized ($E \parallel N_m$) in a TEM_{00} mode ($M^2_{x,y} < 1.05$). The polarization was naturally-selected by the gain anisotropy [28].

Using the SWCNT-SA, the laser generated a maximum average output power P_{out} of 1.37 W at 1932-1944 nm (multi-peak spectrum) with a slope efficiency $\eta = 41\%$ with respect to the absorbed pump power P_{abs} . The laser threshold was at $P_{\text{abs}} = 1.3 \text{ W}$ and the optical-to-optical efficiency with respect to the incident power η_{opt} amounted to 21%. The conversion efficiency with respect to the continuous-wave (CW) operation mode η_{conv} (when the SA was removed from the cavity) reached 53%. For both graphene-SA and SESA, the performance of the laser was inferior resulting in the maximum average output power of 0.70 W with $\eta = 26\%$ and 0.54 W with $\eta = 21\%$, respectively. In addition, the upper limit for stable Q-switching for these SAs was lower, at $P_{\text{abs}} \sim 4 \text{ W}$. Typical spectra of the laser emission in the CW and PQS regime of the Tm-laser are shown in figure 3(b). The multi-peak spectral behavior (1928-1936 nm for graphene-SA and 1926-1943 nm for SESA) is related to etalon effects arising from small separations between the optical elements.

The relevant pulse characteristics, namely the pulse duration τ determined at full width at half maximum (FWHM), pulse repetition frequency (PRF), pulse energy $E_{\text{out}} = P_{\text{out}}/\text{PRF}$ and peak power $P_{\text{peak}} = E_{\text{out}}/\tau$, are shown in figure 4 versus P_{abs} . These values measured at the maximum studied P_{abs} are compared in table 2 for the studied SAs. For all SAs, the pulse characteristics are strongly dependent on P_{abs} due to the dependence of the modulation depth on the intracavity laser intensity [31]. The SWCNT-SA provides superior output characteristics of the PQS Tm-laser as compared to graphene-SA and SESA at any level of the absorbed pump power. As reference, at $P_{\text{abs}} = 3.9 \text{ W}$, the SWCNT PQS laser generated 55 ns / 5.4 μJ pulses at PRF = 195 kHz, compared to 61 ns / 1.1 μJ pulses at 498 kHz for SESA and 123 ns / 3.1 μJ pulses at 230 kHz for graphene-SA. At the maximum studied P_{abs} , sub-50 ns pulses were achieved with SWCNTs and, consequently, the peak power exceeded 100 W which is ~ 5 times higher than that for the SESA.

The oscilloscope traces of the single Q-switched pulses and the corresponding pulse trains recorded at the reference $P_{\text{abs}} = 3.9 \text{ W}$ are shown in figure 5. For the SWCNT-SA, the intensity instabilities in the pulse train were $< 10\%$ and the *rms* pulse-to-pulse timing jitter did not exceed 7%. Similar characteristics were detected for the SESA within the range of stable Q-switching while for the graphene-SA the Q-switching instabilities were more pronounced.

No damage of the SWCNT-SA was observed up to the maximum studied pump power, which provides an estimation for the LIDT of at least 25 MW/cm^2 for ns pulses (according to the calculated intracavity peak on-axis laser intensity on the SA).

Employing the SWCNT-SA for Q-switching of the Tm-laser, the pulse duration (sub-100 ns) is significantly shorter as compared to previous works on bulk $\sim 2 \mu\text{m}$ lasers PQS with carbon nanostructures (graphene and SWCNTs) for which the pulse durations were typically in the range from few hundreds of ns to few μs , see Refs. from [14] and [26] for detailed

comparison. This short pulse duration resulted in the maximum peak power (~100 W) achieved so far for any near-IR bulk laser PQS by carbon nanostructures. What about the semiconductor SAs, a reflection-type SA (SESAM) was employed in [32] resulting in generation of very short but low-energy pulses (2.4 ns / 0.11 μ J) mostly due to the larger modulation depth of the used SA ($\alpha'_s = 5\%$) as compared to the present study.

Recently, SWCNT-, graphene- and semiconductor SAs have been employed for PQS of compact holmium lasers based on Ho:YAG ceramics and operating at ~2.09 μ m [29,33], and a superior performance of SWCNT-SA was demonstrated for this type of lasers, supporting the conclusions of the present work. The possibility for SWCNT-SA to operate at even longer wavelengths, at ~2.13 μ m, was proved with the “vibronic” Tm:KLuW laser in [26].

The advantage of the SWCNT-SA over graphene-SA is the larger fraction of the saturable to the total small-signal absorption α'_s/α' (table 1), or, equivalently, larger modulation depth and simultaneously lower insertion loss of the SA. Consequently, this leads to the generation of shorter pulses with higher energies, together with higher laser efficiency (see figure 3 and figure 4). A frequently claimed possibility to increase the modulation depth of the graphene-SA is the increase of the number of carbon layers. However, this leads to a significant increase of the scattering loss at the layer-to-layer interfaces and, thus, the ratio α'_s/α' drops even further. These arguments explain the generation of longer and less energetic pulses with graphene-SA (table 2), and the lower η_{conv} .

The advantages of the SWCNT-SA over the SESA are the lower saturation fluence (intensity), table 1, and weaker sensitivity to heating by the residual pump. The first advantage means easier bleaching of the SA. In the case of microchip lasers where the size of the laser mode is determined by the thermal lens and it is normally rather small ($w_L = 50...100 \mu$ m), the difference in I_{sat} has less impact on the output characteristics. The second advantage is critical for power scaling and also to reach short pulse durations and high pulse energies which depend on the pump level in the case of “fast” SAs, as shown in figure 4. First, the individual nanotubes are randomly oriented in the film which averages their nonlinear response to the polarized laser radiation and makes the SWCNT-SA almost insensitive to additional disorientations caused by the thermal expansion. Second, the heat transfer in the SWCNT / PMMA film is unidirectional (towards the substrate). The opposite occurs in the SESA, which requires an additional heat sink because of absorption in the GaAs substrate. Finally, the unwanted absorption of SWCNT-SA at the pump wavelength is much weaker than that of the SESA.

Further improvements of the pulse characteristics of ~2 μ m lasers PQS by SWCNTs are possible by increasing the modulation depth of the SA, e.g., by variation of the concentration of nanotubes in the film (in the present work, the modulation depth was selected to equal α'_s of the SESA and SWCNT-SA for a proper comparison). This may lead to the generation of pulses with few ns duration and peak powers of few kW. The SWCNT/PMMA film can also be directly deposited on the end face of the AE providing an extreme compactness of the laser. Power scaling of SWCNT PQS ~2 μ m lasers is expected to provide pulsed operation at frequencies in the MHz-range.

SWCNT-SAs are also very promising for the use in PQS ~2 μ m waveguide lasers where SESAs cannot be easily implemented. Such SWCNT-SAs can be designed as transmission-type devices [34] or deposited on the top surface of the waveguide for evanescent field interaction [35].

5. Conclusion

In conclusion, a direct comparison of “fast” transmission-type SAs based on carbon nanostructures (SWCNTs and graphene with few carbon layers) and a commercial semiconductor SA indicated the superior performance of the SWCNT-SA for passive Q-

switching of ~ 2 μm (thulium) lasers. This absorber is well suited for the development of miniature nanosecond eye-safe lasers operating at high PRFs ranging from hundreds of kHz to few MHz. The SWCNT-SA offers the benefits of high saturable loss, low saturation fluence, ultrafast recovery time, reasonable LIDT and weak sensitivity to heating, as well as easy, size-scalable and reliable fabrication technology. Further improvements seem possible by direct deposition of the SWCNT film onto the surfaces of various optical elements in the laser cavity. These characteristics make the SWCNT-SA a viable alternative to the commercially available semiconductor SAs which are rare at ~ 2 μm .

Acknowledgments

This work was supported in part by the Spanish Government under project MAT2013-47395-C4-4-R, TEC 2014-55948-R and by the Generalitat de Catalunya under project 2014SGR1358. F.D. acknowledges additional support through the ICREA academia award 2010ICREA-02 for excellence in research. X.M. acknowledges support from the European Union's Horizon 2020 research and innovation programme under grant agreement No 654148 Laserlab-Europe and under the Marie Skłodowska-Curie grant agreement No 657630. P. L. acknowledges support from the Government of the Russian Federation (Grant 074-U01) through ITMO Post-Doctoral Fellowship scheme.

References

- [1] Kaminskii A A 2007 *Laser & Photon. Rev.* **1** 93-177
- [2] Zayhowski J J and Dill III C 1994 *Opt. Lett.* **19** 1427-9
- [3] Braun B, Kärtner F X, Zhang G, Moser M and Keller U 1997 *Opt. Lett.* **22** 381-3
- [4] Liu J, Petrov V, Zhang H and Wang J 2007 *Appl. Phys. B* **88** 527-30
- [5] Loiko P, Serres J M, Mateos X, Yumashev K, Yasukevich A, Petrov V, Griebner U, Aguiló M and Díaz F 2016 *Opt. Lett.* **41** 2620-3
- [6] Dong J, Ueda K, Shirakawa A, Yagi H, Yanagitani T and Kaminskii A A 2007 *Opt. Express* **15** 14516-23
- [7] Spühler G J, Paschotta R, Kullberg M P, Graf M, Moser M, Mix E, Huber G, Harder C and Keller U 2001 *Appl. Phys. B* **72** 285-7
- [8] Butler A C, Spence D J and Coutts D W 2012 *Appl. Phys. B* **109** 81-8
- [9] Yu H, Petrov V, Griebner U, Parisi D, Veronesi S and Tonelli M 2012 *Opt. Lett.* **37** 2544-6
- [10] Loiko P, Serres J M, Mateos X, Yumashev K, Yasukevich A, Petrov V, Griebner U, Aguiló M and Díaz F 2015 *Opt. Lett.* **40** 5220-3
- [11] Bao Q, Zhang H, Wang Y, Ni Z, Yan Y, Shen Z X, Loh K P and Tang D Y 2009 *Adv. Funct. Mater.* **1** 3077-83
- [12] Xing G, Guo H, Zhang X, Sum T C and Huan C H A 2010 *Opt. Express* **18** 4564-73
- [13] Cho W B *et al* 2010 *Adv. Funct. Mater.* **20** 1937-43
- [14] Serres J M, Loiko P, Mateos X, Yumashev K, Griebner U, Petrov V, Aguiló M and Díaz F 2015 *Opt. Express* **23** 14108-13
- [15] Gaponenko M S, Onushchenko A A, Kisel V E, Malyarevich A M, Yumashev K V and Kuleshov N V 2012 *Laser Phys. Lett.* **9** 291-4
- [16] Serres J M *et al* 2016 *Opt. Mater. Express* **6** 3262-73
- [17] Wu K, Zhang X, Wang J, Li X and Chen J 2015 *Opt. Express* **23** 11453-61
- [18] Luo Z *et al* 2014 *IEEE J. Sel. Top. Quantum Electron.* **20** 1-8
- [19] Kong L, Qin Z, Xie G, Guo Z, Zhang H, Yuan P and Qian L 2016 *Laser Phys. Lett.* **13** 045801-1-5
- [20] Liu C, Ye C, Luo Z, Cheng H, Wu D, Zheng Y, Liu Z and Qu B 2013 *Opt. Express* **21** 204-9

- [21] Ugolotti E *et al* 2012 *Appl. Phys. Lett.* **101** 161112-1-4
- [22] Cho W B *et al* 2009 *Opt. Express* **17** 11007-12
- [23] Wang Q, Teng H, Zou Y, Zhang Z, Li D, Wang R, Gao C, Lin J, Guo L and Wei Z 2012 *Opt. Lett.* **37** 395–7
- [24] Xie G Q, Ma J, Lv P, Gao W L, Yuan P, Qian L J, Yu H H, Zhang H J, Wang Y J and Tang D Y 2012 *Opt. Mater. Express* **2** 878–83
- [25] Feng T L *et al* 2013 *Laser Phys. Lett.* **10** 095001-1-6
- [26] Loiko P, Mateos X, Choi S Y, Rotermund F, Serres J M, Aguiló M, Díaz F, Yumashev K, Griebner U and Petrov V 2016 *J. Opt. Soc. Am. B* **33** D19-D27
- [27] Serres J M, Mateos X, Loiko P, Yumashev K, Kuleshov N, Petrov V, Griebner U, Aguiló M and Díaz F 2014 *Opt. Lett.* **39** 4247-50
- [28] Petrov V, Pujol M C, Mateos X, Silvestre Ò, Rivier S, Aguiló M, Solé R, Liu J, Griebner U and Díaz F 2007 *Laser & Photonics Rev.* **1** 179-212.
- [29] Lan R *et al* 2016 *Appl. Opt.* **55** 4877-87
- [30] Wildöer J W G, Venema L C, Rinzler A G, Smalley R E and Dekker C 1998 *Nature* **391** 59-62
- [31] Yasukevich A S *et al* 2017 *Opt. Commun.* **389** 15-22
- [32] Gaponenko M, Kuleshov N and Südmeyer T 2016 *IEEE Photon. Technol. Lett.* **28** 147-50
- [33] Lan R, Mateos X, Wang Y, Serres J M, Loiko P, Li J, Pan Y, Griebner U and Petrov V 2017 *Opt. Express* **25** 4579-84
- [34] Kifle E *et al* 2017 *Opt. Lett.* **42** 1169-72
- [35] Kim J W, Choi S Y, Yeom D I, Aravazhi S, Pollnau M, Griebner U, Petrov V and Rotermund F 2013 *Opt. Lett.* **38** 5090-3

Table 1 Parameters* of the studied SAs, at $\sim 2 \mu\text{m}$ [13,21,22,29].

SA	α' , %	α'_S , %	α'_S/α'	F_{sat} , $\mu\text{J}/\text{cm}^2$	I_{sat} , MW/cm^2	τ_{SA} , ps
SESA	1.10	0.55	~ 0.50	300	23	13
SWCNT	2.45	0.50	0.206	9.5**	7 ± 1	0.25, 1.2
Graphene	5.70	0.24	0.042	50***	1 ± 0.2	0.2, 1.5***

* α' – small-signal absorption, α'_S – saturable absorption, F_{sat} – saturation fluence, I_{sat} – saturation intensity, τ_{SA} – recovery time of initial absorption

**At $1.3 \mu\text{m}$, for 100 fs pulses

***At $1.04 \mu\text{m}$, for 200 fs pulses

Table 2 Comparison of the best output characteristics* of the Tm:KLuW laser PQS by SESA, SWCNT-, and graphene-SA.

SA	P_{out} , mW	η , %	η_{conv} , %	τ , ns	E_{out} , μJ	PRF, kHz	P_{peak} , W
SESA	539	21	26	61	1.1	498	18
SWCNT	1360	41	53	48	5.5	250	114
graphene	704	26	34	123	3.1	230	25

* P_{out} – average output power, η – slope efficiency, η_{conv} – Q-switching conversion efficiency, τ – pulse duration (FWHM), E_{out} – pulse energy, PRF – pulse repetition frequency, P_{peak} – peak power

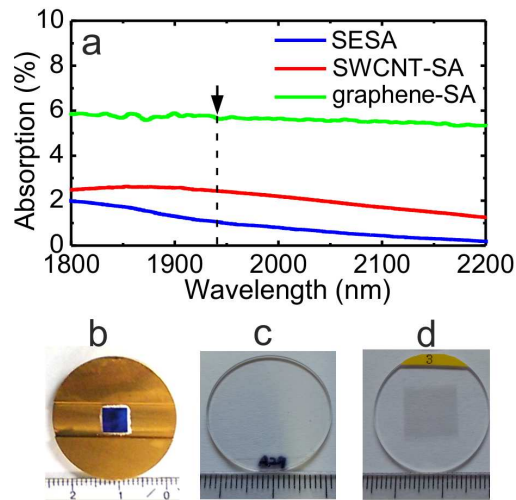


Figure 1 Small-signal absorption in the spectral range of emission of Tm^{3+} and Ho^{3+} lasers (a) and photographs (b-d) of SESA, SWCNT-SA and graphene-SA, respectively. The Arrow in (a) indicates the emission wavelength of the studied Tm laser.

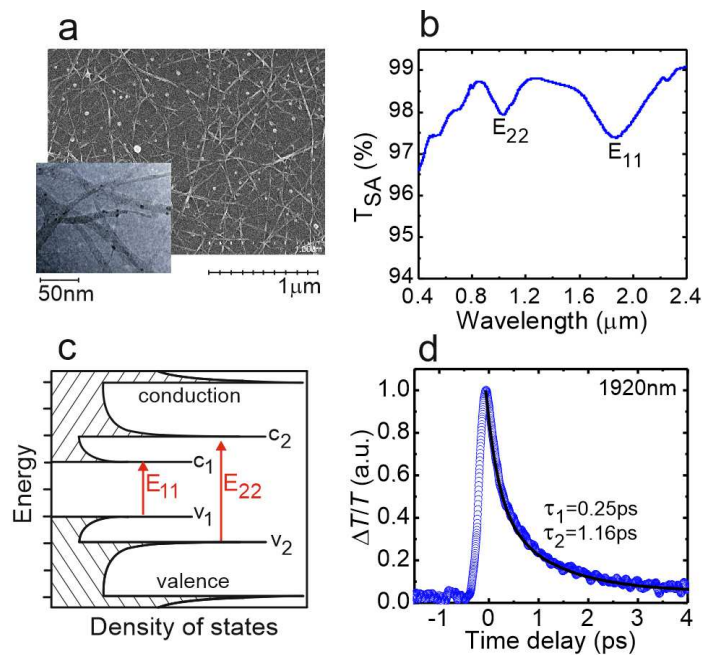


Figure 2 Characterization of the SWCNT-SA: (a) microscope images of the nanotubes; (b) small-signal absorption spectrum; (c) scheme illustrating the band structure and the allowed optical transitions for SWCNTs; (d) recovery of the initial absorption measured by the pump-probe technique, τ_1 and τ_2 are the characteristic times of the bi-exponential fit.

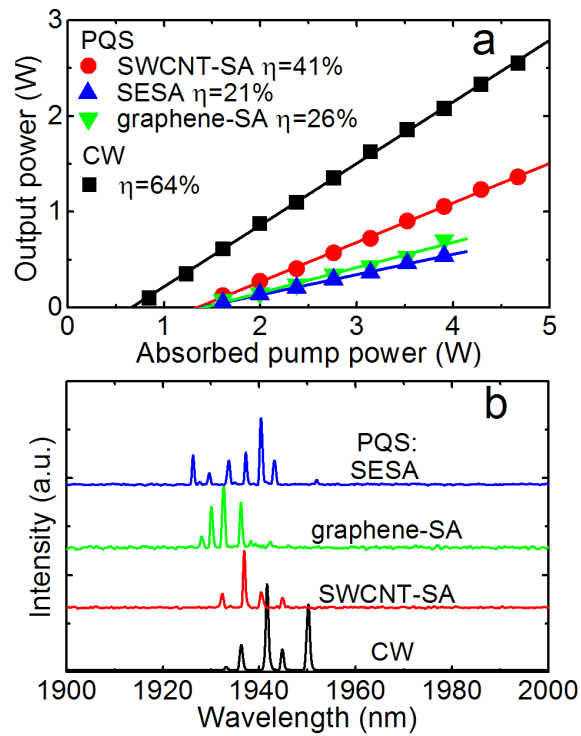


Figure 3 Tm:KLuW laser PQS with SESA, SWCNT-SA and graphene-SA: (a) input-output dependences, *lines* represent the fits for the slope efficiency (η) calculation, (b) typical laser emission spectra at $P_{\text{abs}} = 3.9$ W.

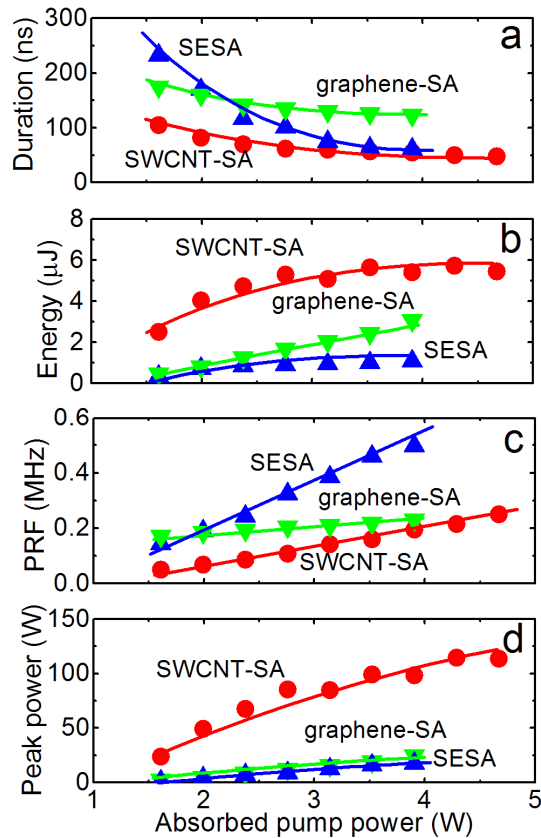


Figure 4 Tm:KLuW laser PQS with SESA, SWCNT-SA and graphene-SA: (a) pulse duration (FWHM), (b) pulse energy, (c) pulse repetition frequency (PRF) and (d) peak power.

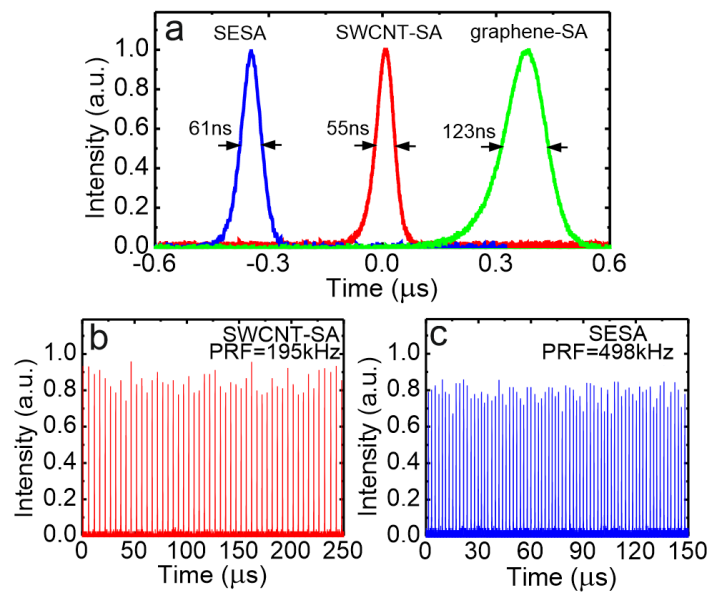


Figure 5 Oscilloscope traces of output pulses of the Tm:KLuW laser PQS with SESA, SWCNT-SA and graphene-SA: single Q-switched pulses (a) and the corresponding pulse trains for SWCNT-SA (b) and SESA (c), $P_{\text{abs}} = 3.9$ W.